Article

Achieving Intensity Distributions of 6 February 2023 Kahramanmaraş (Türkiye) Earthquakes from Peak Ground Acceleration Records

Aydın Büyüksaraç [1,*] , Ercan Işık [2] , Özcan Bektaş [3] and Fatih Avcil [2]

1   Çan Vocational School, Çanakkale 18 Mart University, Çanakkale 17400, Türkiye
2   Department of Civil Engineering, Bitlis Eren University, Bitlis 13100, Türkiye; eisik@beu.edu.tr (E.I.); favcil@beu.edu.tr (F.A.)
3   Department of Geophysical Engineering, Sivas Cumhuriyet University, Sivas 58140, Türkiye; obektas@cumhuriyet.edu.tr
*   Correspondence: absarac@comu.edu.tr

Abstract: On 6 February 2023, two large earthquakes struck southern Türkiye on the same day, resulting in a considerable loss of life and property damage over a large region that included 11 cities. After these disasters, there was a requirement to define the soil-related intensity distribution, aside from manufacturing defects caused by buildings. The modified Mercalli intensity (MMI) scale results in the same intensity value (XI) when decimal values are not mathematically considered, even though the fundamental data in the AFAD and USGS sources differ. In this study, an equation based on the MMI–PGA relationship was obtained and tested with ten previously developed equations to calculate the earthquake intensity. Seven of these selected equations, depending on the earthquake magnitude, were calculated comparatively. The equation most compatible with the earthquakes that occurred on 6 February 2023 was obtained in this study. In addition, it was decided that three similar equations could also be used. Intensity distribution maps were created according to the calculated MMI values. In this way, it has been observed that different earthquake intensity values are more sensitive, reliable, objective, and sustainable.

Keywords: earthquake intensity; intensity scale; damage distribution; sustainable assessment

1. Introduction

Recent earthquakes in Kahramanmaraş (Türkiye), Marrakesh (Morocco), Herat (Afghanistan), and similar earthquakes have once again demonstrated the importance of studies on this subject. One of the most important natural disasters that cause the destruction of an entire region is earthquakes. The concepts of magnitude and intensity are used to reveal the destructive nature of earthquakes. Before the invention of devices that allow measuring the energy released by earthquakes, the destructive effects of earthquakes were evaluated by their effects on people and structures. In this context, the concept of earthquake intensity was used to reveal the effects of earthquakes historically [1–7]. Any earthquake's intensity (I) can be measured based on how people feel it, whether there is structural damage, and whether there are any surface-level occurrences like cracks and fractures in the earth. It is a useful assessment that was developed to gauge the intensity of ground shaking and assess the damage during times when instrumental measurements were not possible. Different intensity scales created by numerous researchers are available. The most widely used of these is the Mercalli intensity scale. The Mercalli scale was created by Giuseppe Mercalli in 1902. It later continued to be measured using the modified Mercalli intensity (MMI) scale [8,9]. This scale consists of 12 intensity levels given with Roman numerals, i.e., I to XII. Scaling is determined depending on the damage and effects of an earthquake. An equivalent intensity map is obtained by determining the intensity values at

various points in an earthquake region and separating the points with the same intensity by contours on the map. The shape of the contours on iso-intensity maps depends on the structure of the region and the characteristics of the earthquake. Although in some earthquakes they appear circular, in others, especially if a fault movement occurs on the earth, they appear as ellipses, extending along the fault direction. By using equivalent intensity maps, the earthquake intensity and macroseismic external focus can be obtained. The intensity of an earthquake is the greatest intensity value (*Io*) detected in the earthquake region. The intensity of an earthquake became comparable to the magnitude of an earthquake after the instrumental recording period. Earthquakes with magnitudes between 1.0 and 5.0 produce insensible-to-moderate intensity effects and have almost the same value on the Mercalli scale. However, above a magnitude of 5.0 and intensity V, both the perceived value and the potential for damage increase. At higher levels, it may reach levels that require damage assessment. Different relations have been developed for the intensity of an earthquake at its focal point, or, in other words, its maximum intensity. Among these, Shebalin's [10] equation gives very accurate results (Equation (1)).

$$Io = 1.5M - 3.5\log h + 3.0 \tag{1}$$

In the equation, *Io* is the maximum intensity, M is the magnitude, and h is the hypocenter of the earthquake. After an earthquake, if the magnitude and hypocenter of the earthquake are known, the maximum intensity at the epicenter of the earthquake can be calculated in this way. Thus, intensity distribution maps and even earthquake hazard maps have been prepared, taking into account the maximum intensity values calculated after earthquakes. For example, earthquake hazard zonation maps in Türkiye were initiated after Türkiye's largest earthquake with $M_w = 7.9$, which occurred in Erzincan in 1939. The first earthquake zonation map was created in 1945 by compiling the damage information caused by earthquakes that occurred in previous years from archives. The maps were updated after major earthquakes that occurred at different times until 1972. This map has been updated by taking into account earthquake catalogues, earthquake epicenter distribution maps, felt maximum intensity maps, and seismotectonic maps. In 1996, the concept of earthquake zonation was completely changed, and a new map was prepared, taking into account earthquake source zones, a statistical evaluation of past earthquake records for each source zone, the maximum earthquake magnitude that the source zones can create, acceleration decay relations, and the largest cumulative probability distribution function of acceleration valid in the specified period for each source zone. Five earthquake zones were determined on this map; the first-degree earthquake zone was defined as regions where the PGA value was equal to or exceeded 0.4 g, and the fifth-degree earthquake zone was defined as non-hazardous regions where the PGA value was lower than 0.1 g. In 2018, this map was updated again and became the version used today, but zonation based on acceleration change was not abandoned. As seen in this chronological process, a method has been developed to move away from criteria based on different life cultures and socio-economic conditions that are not differentiated in the MMI scale by taking into account more objective conditions in calculating the earthquake intensity. Of course, the fact that the acceleration value is a very important parameter that also includes ground conditions played an important role in the formation of these calculations and subsequent maps. Otherwise, the distribution of damage after earthquakes and, hence, the intensity assessment may not allow for an objective assessment. Although the MMI scale continues to be used in calculating intensity distributions, correlations that base intensity values on PGA values are also used very efficiently with this approach. Many studies have been conducted comparing the relationship between the PGA and earthquake intensity [11–23]. A large number of studies have been conducted, especially on California earthquakes [24–28]. In recent years, correlations based on local-scale comparisons have been developed. For example, Karim and Yamazaki [29] for Japanese data; Wu et al. [30] for Taiwan; Kaka and Atkinson [31] for eastern North America; Tselentis and Danciu [32] for Greek earthquakes; Gama Garcia and Gomez Bernal [33] and Sørensen et al. [34] for Guer-

rero, Mexico; Linkimer [35] for Costa Rica, Faenza, and Michelini [36] for Italy; Bayrak [37] for Türkiye; Ardeleanu et al. [38] for Vrancea Region, Romania; Cilica and Baker [39] for Chilean earthquakes and subduction zones; Hariyanto et al. [40] for multi-event earthquake data; Konovalov et al. [41] for Sakalin Island; Anugrayanti et al. [42] for Mamasa; and Tian et al. [43] for China are some of the developed correlations.

During the two major earthquakes that occurred on the same day in the south of Türkiye on 6 February 2023, significant losses of life and property happened in an extensive area covering 11 cities. There is a necessity to objectively evaluate the intensity distribution that occurs after these earthquakes, other than structural failure caused by buildings. Developing a correlation for assessment and comparing it with previous research are the main objectives of this study. In the paper, primarily, comprehensive information is given about the 6 February 2023 Kahramanmaraş earthquakes, which are called the disaster of the century in Türkiye. The measured current PGA values of these earthquakes, independent of each other, were compared with the PGA values predicted in the current earthquake hazard map in Türkiye. In addition, design spectra were compared for 11 different provinces affected by the earthquake. Intensity distributions for both earthquakes were obtained separately. It will be one of the first studies in which intensity distributions are obtained by taking both earthquakes into account in the entire earthquake region.

This study is important in terms of revealing the calculability of earthquake intensity estimation, which is equivalent to assessing the effects of earthquakes from acceleration, which is a continuously measurable parameter, before an earthquake occurs in order to identify the risks that cities may incur from existing earthquake hazards. Existing building stock and newly constructed buildings face sustainability problems from natural and environmental disasters. Therefore, it is of great importance to take sustainability principles into consideration in the design and construction processes of buildings. A realistic determination of the risk caused by seismic hazards will increase the earthquake resistance of structures and make them safer against earthquakes or other external factors. In the article, the earthquake intensity, which is of great importance for local people to manage the processes of natural disasters in the future, is analyzed through the example of the earthquakes that occurred on 6 February 2023 in Türkiye.

2. Kahramanmaraş Earthquakes on 6 February 2023

Kahramanmaraş, located in the south of Türkiye, is one of the settlements located in the Eastern Anatolian Fault Zone (EAFZ). The city, which has been exposed to major earthquakes in the past, is on the fifth segment of the EAFZ, one of the well-known segments. In this segment, where no major earthquake had occurred since 1513, an earthquake with a magnitude of $M_w = 7.7$ occurred in the very early hours of the morning on 6 February 2023. Approximately 9 h after this earthquake, a second earthquake with a magnitude of $M_w = 7.6$ occurred in the same region, north of the focal point of the first earthquake. These two earthquakes and about 40,000 aftershocks caused a huge disaster in the region (Figure 1). More than 50,000 people in Türkiye and approximately 5000 people in Syria lost their lives in the earthquake, which also affected the north of Syria. More than 230,000 buildings were either destroyed or so severely damaged that they were uninhabitable. Information such as the magnitude, location, and focal depth of both earthquakes is summarized in Table 1 based on the AFAD (Türkiye) and USGS (USA) sources. Although the values from both sources are very close to each other, the earthquake magnitudes and focal depths are different. When the maximum intensity values at the focal centers are calculated using the Shebalin [10] relation, it is understood that the intensity of both earthquakes was XI.
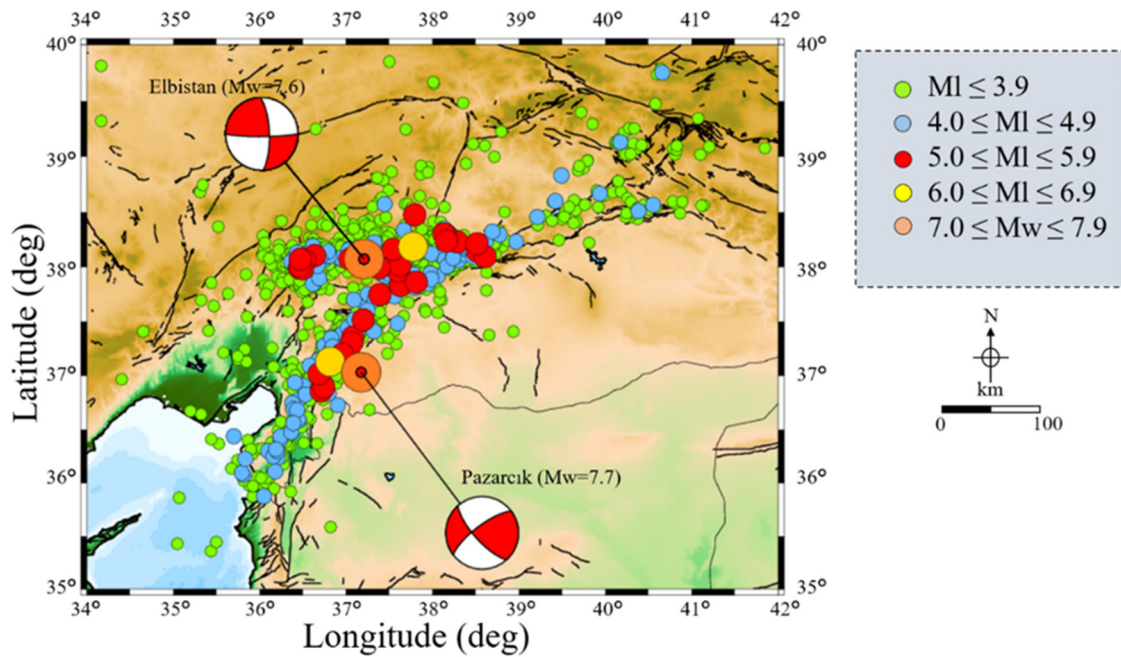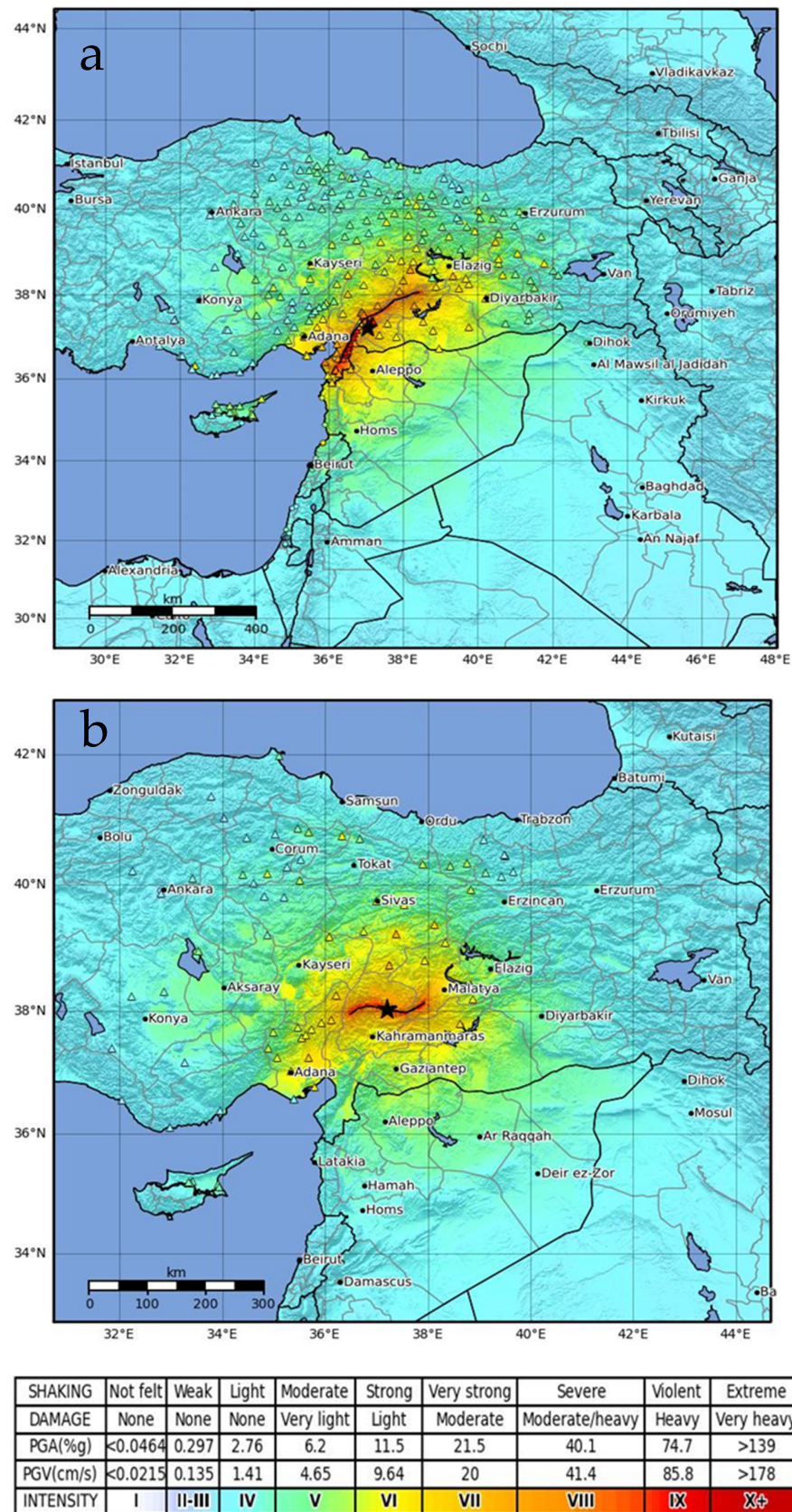
Figure 1. Epicenter distribution of the Pazarcık (Kahramanmaraş) earthquake (M_w = 7.7) and Elbistan (Kahramanmaraş) earthquake (M_w = 7.6) and their aftershocks from 6 February 2023 to 10 February 2023. Magnitude levels of the events are depicted with different symbols. The fault plane solutions of main shocks are taken from the AFAD website. The seismicity catalogue information is obtained from the Kandilli Observatory and Earthquake Research Institute.

Table 1. Information obtained from two different sources about the earthquakes that occurred on 6 February 2023.

Date/Time	Coordinates	Location	Magnitude (M_w)	Depth (km)	Source	Eq. Intensity
6 February 2023 04:17:34 (TSI)	37.288° N 37.043° E	Pazarcık (Kahraman-maraş)	7.7	8.60	AFAD	XI (11.28)
	37.225° N 37.021° E		7.8	10.0	USGS	XI (11.2)
6 February 2023 13:24:47 (TSI)	38.089° N 37.239° E	Ekinözü, Elbistan (Kahraman-maraş)	7.6	7.0	AFAD	XI (11.44)
	38.024° N 37.203° E		7.5	10	USGS	X–XI (10.75)

Even though the fundamental data from the USGS and AFAD sources disagree, the MMI scale yields the same intensity value when decimal numbers are ignored mathematically. For the first earthquake, according to the AFAD source, the focal depth was measured at 8.6 km and the magnitude was M_w = 7.7. According to the USGS source, the focal depth was measured at 10 km and the magnitude at M_w = 7.8. Although a shallower focal depth and a smaller earthquake were measured for the first earthquake in the AFAD source, both sources gave approximately the same value mathematically. For the second earthquake, according to the AFAD and USGS sources, an earthquake with a focal depth of 7 km and 10 km and a magnitude of M_w = 7.6 and M_w = 7.5 was, respectively, measured. The AFAD source mathematically gave a greater intensity value. However, when these values were rounded, the intensity was consistent with XI. These results are also in agreement with the MMI–magnitude relationship.

When the intensity distribution maps made by the USGS are examined, it is seen that the intensity calculation is compatible with the results obtained at the focal points (Figure 2).

SHAKING	Not felt	Weak	Light	Moderate	Strong	Very strong	Severe	Violent	Extreme
DAMAGE	None	None	None	Very light	Light	Moderate	Moderate/heavy	Heavy	Very heavy
PGA(%g)	<0.0464	0.297	2.76	6.2	11.5	21.5	40.1	74.7	>139
PGV(cm/s)	<0.0215	0.135	1.41	4.65	9.64	20	41.4	85.8	>178
INTENSITY	I	II-III	IV	V	VI	VII	VIII	IX	X+

Figure 2. Intensity distribution maps created by USGS: (**a**) Mw = 7.8; (**b**) M_w = 7.5. Δ: accelerometers; (star) epicenter. Scaled based on Worden et al. [28]. (https://earthquake.usgs.gov/earthquakes/eventpage/us6000jlqa/shakemap/intensity) (accessed on 23 November 2023) [44].

The Kahramanmaraş earthquakes, which occurred independently of each other 9 h apart, caused great destruction to structures with many different load-bearing systems. As a result of the earthquakes, the most structural destruction and loss of life occurred in the Hatay, Kahramanmaraş, and Adıyaman provinces. Particularly in rural areas, masonry structures, which are the dominant building stock, reinforced concrete structures, which are the dominant city building stock, mosques and minarets, transportation, and infrastructure facilities have suffered huge demolitions, and as a result, huge economic losses have occurred [45–47]. The destruction caused these earthquakes to be recorded as the most devastating earthquakes in the country. It is stated that the main reason for building collapses is a failure to fully implement earthquake-resistant building design principles [48–54].

3. Method

Ground motion-to-intensity conversion equations are predictive equations that describe the empirical relationship between instrument-measured ground motions, such as the peak ground acceleration (PGA), the peak ground velocity (PGV), and the observed intensities (MMIs). These are used to create maps of intensities calculated from measured ground motions shortly after a major earthquake, as opposed to creating traditional intensity distribution maps determined through human observations. Thus, the earthquake hazard in terms of intensity scale is defined. This information can be considered an important reagent to understand the active fault effect and the share of ground conditions, building quality, and strength information in the intensity distribution.

3.1. Strong Motion Database

Although calculating the maximum intensity value according to the focal point with Equation (1) gives accurate results, the intensity distribution in the places where earthquakes are felt can also be calculated using the records of acceleration stations commonly found in Türkiye. Türkiye National Strong Motion Observation Network was established in 1973 to record the strong motion of earthquakes occurring in the country. Ground acceleration records, which were made with analogue recorders until the 1990s, have also been recorded digitally since 2013. Overall, 950 accelerometer recording stations, which receive real-time recordings, are located mainly along the North Anatolian Fault Zone, East Anatolian Fault Zone, and Aegean Graben systems, which have produced or have the potential to produce major earthquakes. Data are transferred from the stations to various communication tools in a continuous fashion and in real time. In the Turkish National Strong Motion Observations data center, it is possible to access all numerical data provided by accelerometer devices from the establishment of the network to the present. The data are presented in ASCII format. Under the header information of each file, there are acceleration values of the components in the "N-S" (north–south), "E-W" (east–west), and "U-E" (vertical) directions. The sampling interval for each record is included in the header information (Sample Interval). The time series of records obtained from digital devices were not subjected to any correction process. Only an axis-shift (off-set) correction was made in the records called raw data. All the data are acceleration values and are in cm/s^2 (gal).

Two major earthquakes that occurred on 6 February 2023 were also recorded by remote stations. During the M_w = 7.7 earthquake, very large acceleration values occurred. The highest acceleration value was recorded as 2039.20 cm/s^2 in Pazarcık (Kahramanmaraş), and the second was 1372.071 cm/s^2 in Hatay. Apart from this, there are a few more records above 1 g in Hatay (Tables 2 and 3). High acceleration values also occurred during the second earthquake (M_w = 7.6), and the highest acceleration value was measured in Göksun (Kahramanmaraş) with 635.44 cm/s^2. The acceleration stations whose data were used during the study are shown in Figure 3.

Table 2. Expected acceleration, measured acceleration, and probability of exceedance at some acceleration stations (M_w = 7.7).

				M_w = 7.7				
				TBEC-2018				1996
Station	Province/District	PGA (cm/s^2)	Repi	DD1	DD2	DD3	DD4	10%
0131	Adana /Saimbeyli	159.77	103.35	0.519	0.262	0.086	0.057	0.1
0213	Adıyaman/Tut	242.28	96.48	0.809	0.440	0.147	0.094	0.4
2104	Diyarbakır/Ergani	116.47	262.22	0.572	0.320	0.137	0.100	0.4
2310	Elazığ/Baskil	60.46	211.7	0.676	0.360	0.138	0.092	0.3
2718	Gaziantep/Islahiye	654.43	48.3	1.061	0.563	0.166	0.107	0.4
3135	Hatay/Arsuz	1372.07	142.15	0.468	0.256	0.106	0.076	0.4
4414	Malatya/Kale	163.84	195.07	0.809	0.451	0.175	0.115	0.4
4614	Kahramanmaraş/Pazarcık	2039.20	31.42	0.853	0.470	0.157	0.100	0.4
6304	Şanlıurfa/Bozova	238.23	130.27	0.339	0.151	0.055	0.037	0.2
7901	Kilis/Centre	53.11	64.7	0.427	0.210	0.079	0.057	0.1
8002	Osmaniye/Bahçe	242.95	43.91	0.719	0.391	0.140	0.095	0.4

Table 3. Expected acceleration, measured acceleration, and probability of exceedance at some acceleration stations (M_w = 7.6).

				M_w = 7.6				
				TBEC-2018				1996
Station	Province/District	PGA (cm/s^2)	Repi	DD1	DD2	DD3	DD4	10%
0131	Adana/Saimbeyli	402.30	101.83	0.519	0.262	0.086	0.057	0.1
0213	Adıyaman/Tut	126.62	68.73	0.809	0.440	0.147	0.094	0.4
2107	Diyarbakır/Çermik	47.61	196.48	0.566	0.316	0.132	0.095	0.4
2308	Elazığ/Sivrice	69.80	185.23	1.101	0.622	0.230	0.145	0.4
2703	Gaziantep/Şahinbey	93.68	115.06	0.340	0.175	0.072	0.052	0.2
3144	Hatay/Hassa	78.11	156.81	1.134	0.603	0.173	0.109	0.4
4406	Malatya/Akçadağ	467.20	70.17	0.857	0.395	0.111	0.073	0.3
4612	Kahramanmaraş/Göksun	635.45	66.68	0.624	0.296	0.086	0.056	0.3
6306	Şanlıurfarfa/Akçakale	36.00	213.7	0.159	0.075	0.028	0.020	0.1
7901	Kilis/Centre	50.91	153.88	0.427	0.210	0.079	0.057	0.1
8003	Osmaniye/Centre	66.60	140.65	0.597	0.311	0.115	0.079	0.4

The Turkish Acceleration Database and Analysis System (AFAD TADAS) website provides the majority of the data in the strong motion database used in this report. Researchers can quickly and easily access and analyze the data in AFAD's Türkiye Earthquake Monitoring and Evaluation Centre via the Internet. Moreover, the AFAD-TADAS makes it possible to store and share the raw data that are used to perform the analyses and that it automatically provides to earthquake researchers. Strong motion data are susceptible to several problems, including digitization distortion, baseline drift, and instrument errors, which can compromise their consistency and accuracy. The TADAS has also processed and corrected raw data using standard procedures and methods, such as applying filters, eliminating outliers, interpolating missing values, etc., to prevent such issues. In this study, measured PGAs were obtained from the TADAS. For the expected PGA values, the Türkiye Earthquake Hazard Map Interactive Web Earthquake application was used. In this

application, seismic parameters can be obtained for different ground motion levels. There are four different ground motion levels: DD-1, DD-2, DD-3, and DD-4. The ground motion level that has a 2% probability of exceedance in 50 years is DD-1, 10% is DD-2, 50% is DD-3, and 68% is DD-4. These earthquake ground motion levels are stated in the currently used earthquake code (TBEC-2018) in Türkiye. There is only one earthquake ground motion level (DD-2) in the previous earthquake hazard map that was used in 1996.
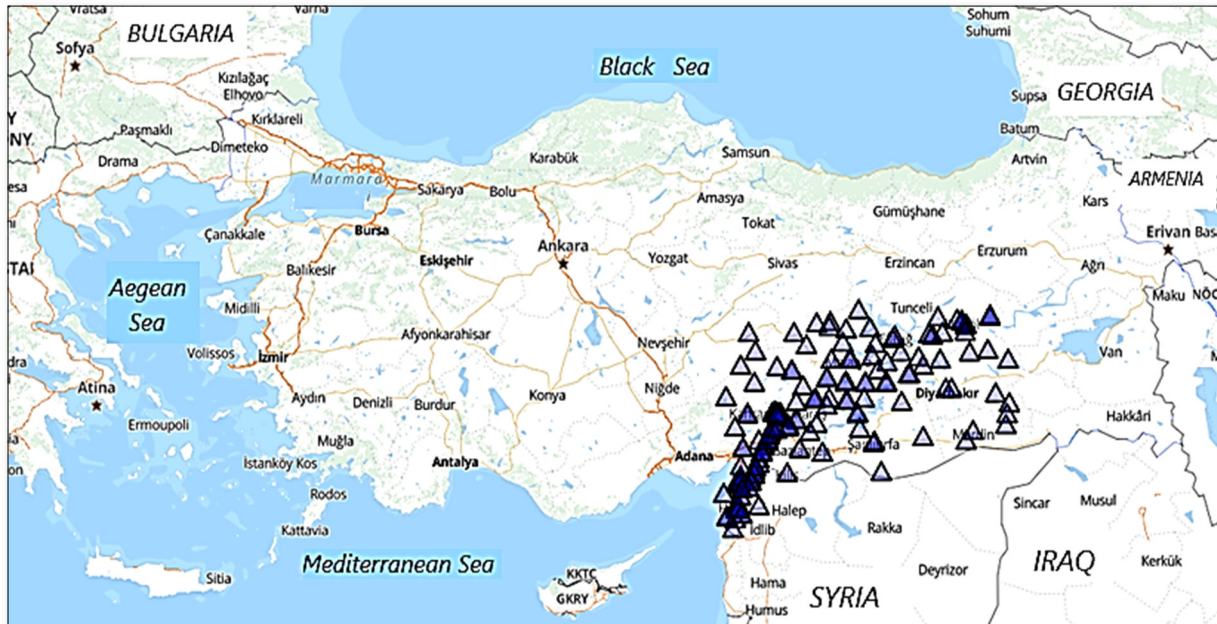
Figure 3. Distribution of acceleration stations used in the study. Triangles shows acceleration station controlled by AFAD.

The peak ground acceleration (PGA) is the most widely used parameter for intensity measures. The PGA is an important parameter for earthquake hazard assessments and gives information about earthquake potential. The PGA is obtained by using attenuation relationships between different parameters, such as the earthquake magnitude, the distance to the epicenter, the local ground conditions, and the focal mechanism. PGA value distribution maps were created for both earthquakes that took place on 6 February 2023 using the acceleration values from 280 records (Figure 4a,b).

3.2. Strong-Ground-Motion-to-Intensity Conversion Equations

In studies conducted by different researchers, the calculation of the intensity distributions of earthquakes according to PGA values was carried out based on experimental relations (Table 4). MMI–acceleration graphs were drawn using acceleration equations obtained from studies conducted in different geographical locations, and their compatibility with the intensity distributions obtained from the February 6 earthquakes in Türkiye was examined (Figures 5 and 6). Some of the correlations were created based on statistical information obtained in accordance with a low intensity distribution. For this reason, correlations were used, taking into account large intensity values. Existing ground motion prediction equations for earthquakes in a subduction zone that occurred in Chile and were defined as mega earthquakes were evaluated as incompatible for Chile, and it was suggested that the new equations produced should be used specifically for Chile within subduction zones [39]. The development of PGA–MMI equations in earthquake hazard definitions has also been a common practice in recent years. For example, in Pandeglang Regency, in one of the subduction zones located in the south of Java Island, earthquake levels based on equations developed due to frequent earthquakes were defined; 37% were determined to be medium-level, and 62% were determined to be high-level earthquake

hazard areas [40]. Similarly, Anugrayanti et al. [42], in their study, developed a scale range between the PGA and MMI obtained after the earthquake in Mamasa (Indonesia) in 2018. The results achieved showed a high level of agreement with the observation-based severity change. In China, long-term PGA records were evaluated, and earthquake hazard maps were created with correlations converted to the MMI scale [43,55]. On the other hand, experimental correlations have been developed for earthquake early warning systems using the strong motion data set for multiple ground motion intensity measurements on Russia's Sakhalin Island [41].
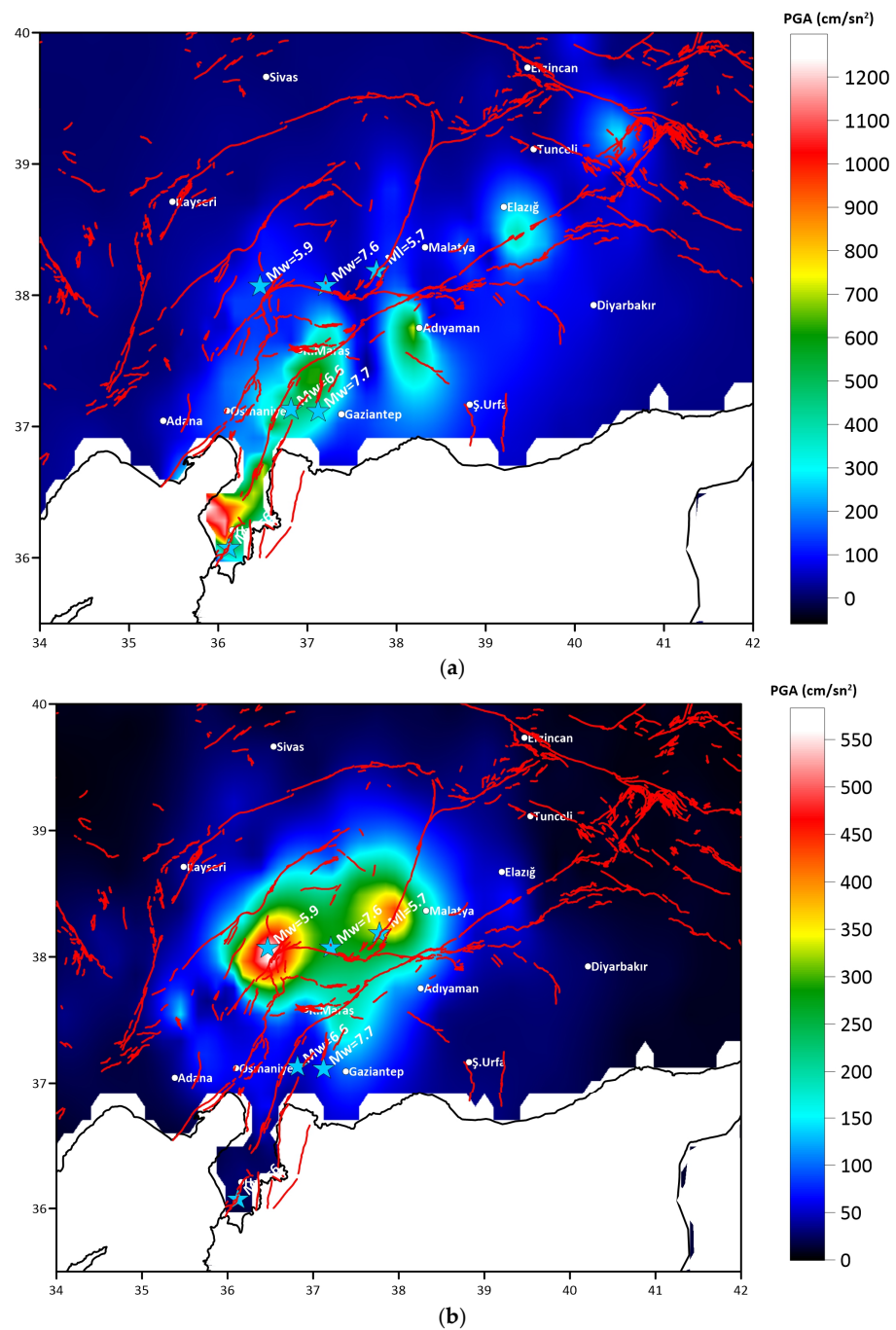
Figure 4. (**a**) PGA value distribution map of the 6 February 2023 Pazarcık–Kahramanmaraş (M_w = 7.7) earthquake. (**b**) Acceleration value distribution map of the 6 February 2023 Elbistan–Kahramanmaraş (Mw = 7.6) earthquake.

Table 4. Logarithmic relationships between acceleration (PGA) and intensity (MMI).

No	Location	Equation	Intensity Range	References
1	Western USA	MMI = 3.00 log (PGAave) + 1.50	All	[9,50,51]
2	Western USA	MMI = 2.33 log (PGAave) + 2.1	All	[56]
3	Western USA	MMI = 3.33 log (PGAave) − 0.47	IV < MMI < X	[11]
4 *	Western USA, Japan, Southern Europe	MMI = 2.86 log (PGAave) + 1.24 MMI = 4.00 log (PGAmax) − 1.00	IV < MMI < X IV < MMI < VIII	[12]
5	Costa Rica	MMI = 3.62 log (PGAave) − 0.90	All	[57]
6 *	California	MMI = 2.20 log (PGAmax) + 1.00 MMI = 3.66 log (PGAmax) − 1.66	MMI < V V < MMI < VIII	[25]
7	California	MMI = (4.36 + 0.71) log (PGA) − (3.88 − 1.76)	All	[23]
8	Taiwan	MMI = 2.00 log (PGA) + 0.7	All	[14,30]
9 *	Costa Rica	MMI = 2.30 log (PGAmax) + 0.92 MMI = 3.82 log (PGAmax) − 1.78 MMI = 2.33 log (PGAave) + 0.76 MMI = 4.60 log (PGAave) − 3.38	II > MMI > V V > MMI > VII II > MMI > V V > MMI > VII	[35]
10	Türkiye	MMI = log (PGA) + 0.427/0.3392	All	[37]
11	This Study	MMI = 3.02 log (PGA) + 1.62	MMI > IX	

* These relations were not used in this study because they were produced for low-intensity earthquakes.
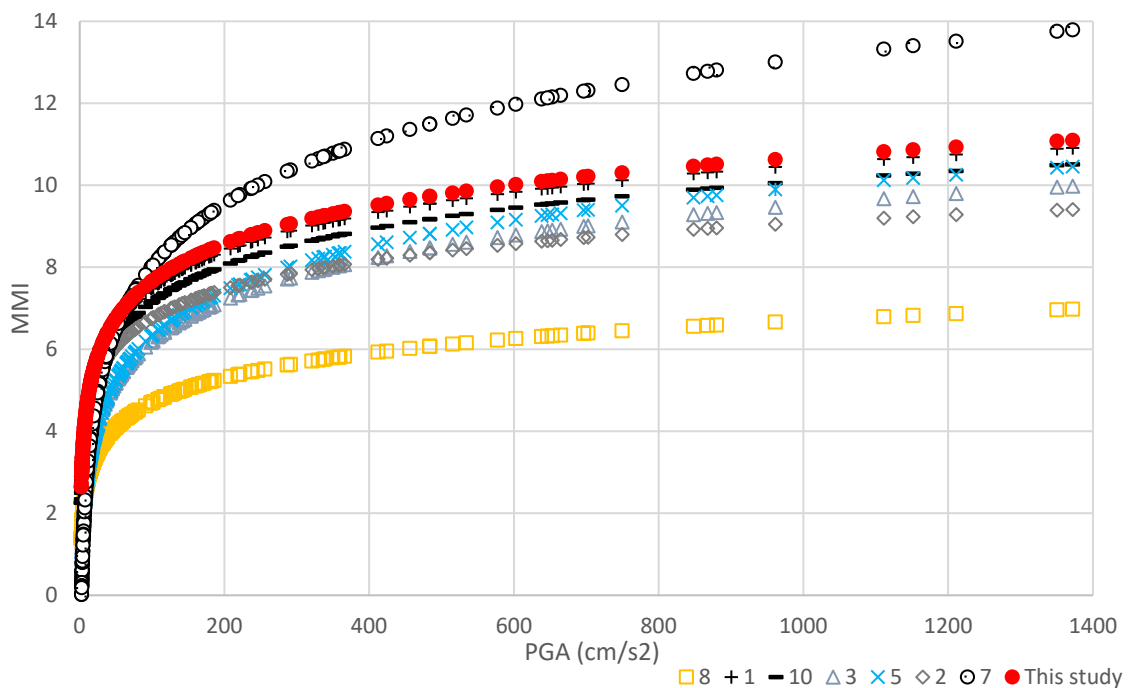
Figure 5. MMI–PGA graphics of the Mw = 7.7 earthquake calculated with different relations. The numbers given were created while taking into account the order in Table 4.
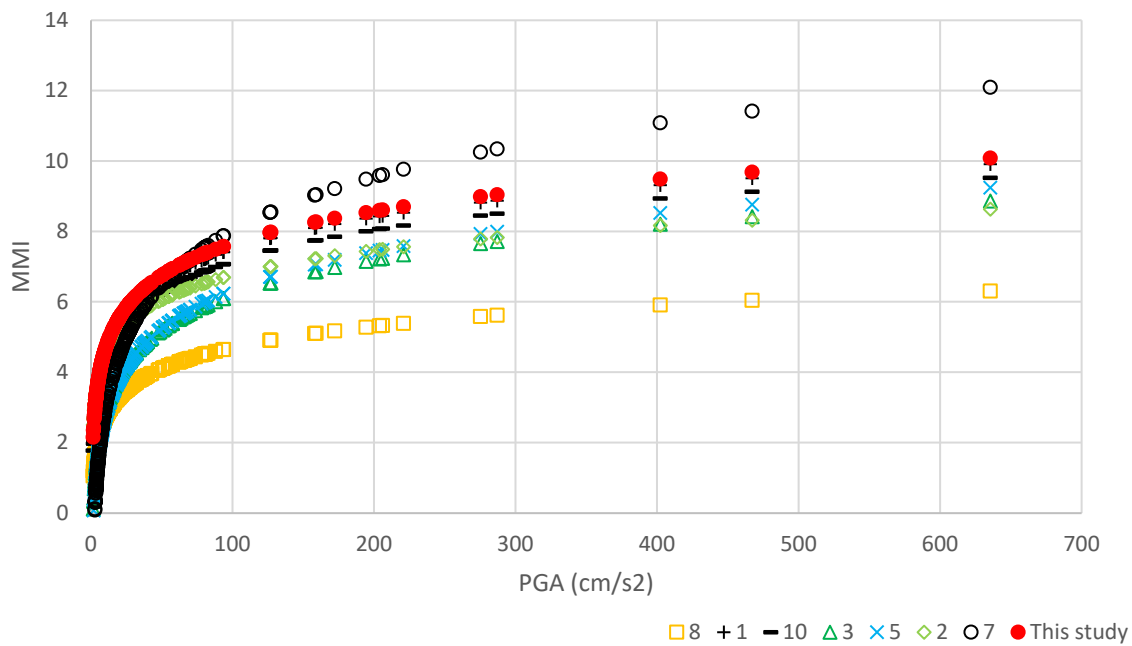
Figure 6. MMI–PGA graphics of the M_w = 7.6 earthquake calculated with different relations. The numbers given were created while taking into account the order in Table 4.

Earthquake intensity, a qualitative parameter that describes the degree of ground vibration and damage caused by an earthquake, is actually a macroscopic scale determined to describe the magnitude of the impact of an earthquake on human communities. For this reason, it is widely used in the evaluation of earthquake effects, loss estimation, and determining the level of structural response. It also helps analyze the recurrence of historical earthquakes in other areas around the world. Traditionally, seismic intensity is obtained by experts who investigate building damage in an area where an earthquake occurred and people's responses to an earthquake. Ground motion parameters, such as the PGA and PGV, which are used as quantitative indexes to define the degree of ground vibration, are generally obtained from the recordings of accelerometers deployed in earthquake regions. Converting ground motion parameters into seismic intensity and the method of creating a conversion equation between them is extremely important in terms of creating intensity distribution maps and quickly assessing loss of life and property [43]. Equation (2) is used to convert the peak ground motion (PGM) (or PGA or PGV) to the earthquake intensity scale (MMI).

$$MMI = C_1 \cdot \log PGM + C_2 \tag{2}$$

Here, C_1 is the slope obtained from the linear regression, and C_2 is the intercept. The opposite of this situation is also possible, and from this correlation pattern, the logPGM value can be calculated from the intensity values of historical earthquakes. In studies conducted by different researchers, the calculation of the intensity distributions of earthquakes according to the acceleration value was carried out based on experimental equations. These equations were mostly created based on the average or maximum acceleration value. Within the scope of this study, Equation (2), based on the c1 and c2 coefficients created by using the pattern in Equation (2), gave a very compatible result depending on the PGA values obtained after the 6 February 2023 earthquakes. The MMI–PGA equations obtained from previous studies and this study are given in Table 4. MMI–PGA graphs were drawn using the acceleration relations obtained from studies conducted in different geographical locations, and their compatibility with the intensity distribution obtained for the February 6 earthquakes was examined (Figures 5 and 6). Some of the correlations were created based on statistical information obtained in accordance with a low-intensity distribution. For this reason, the correlations were used while taking into account large intensity values.

4. Discussion

The level of damage during earthquakes could increase remarkably due to the double-resonance phenomenon that occurs when the fundamental vibration frequencies of structures approach the natural frequencies of soil. For this reason, when defining the damage distribution after earthquakes, the presence of soil-related effects should first be investigated along with structural defects. The potential damage that double-resonance effects can cause to multi-storey buildings was highlighted in detail by Gallipoli et al. [58]. Gallipoli et al. [59] recorded an acceleration greater than 5g% close to a two-story reinforced concrete building in Bagnoli (Naples, Italy) during a major displacement test. The expected PGA values in the places where the acceleration stations whose data were used in this study during the February 6 earthquakes are located are given in Tables 2 and 3, and the PGA values and probability of exceedances measured during the earthquakes are stated. At the same time, a comparison was made between the measured and predicted values for each station in the 11 provinces most affected by the earthquakes and where the largest PGA values were measured. As can be understood from these data, most of the damage observed from the February 6 earthquakes was based on soil-related effects. Of course, the defects of the structures built without taking into account the ground conditions are also added to this. According to TBEC-2018, the horizontal earthquakes obtained by considering the ZC soil class for the selected settlements of the design earthquakes (DD-1 and DD-2) with a probability of exceeding them in 50 years are 2% (recurrence period 2475 years) and 10% (recurrence period 475 years). A comparison of the design spectrum is given in Figure 7a,b, respectively.

In the stations where the largest PGA values were measured for the first earthquake (Mw = 7.7), they were exceeded for five earthquake stations in the 1996 Türkiye Earthquake Zones Map. It is seen that the PGA values predicted for DD-2, which is the standard design ground motion level in TBEC-2018, do not meet the PGA values measured at the Gaziantep/Islahiye, Hatay/Arsuz, Kahramanmaraş/Pazarcık, and Şanlıurfa/Bozova earthquake stations. For DD-1, which is the largest earthquake ground motion level for the geographical locations where these stations are located, the PGA values measured for Arsuz (Hatay) and Pazarcık (Kahramanmaraş) were higher than the recommended PGA values. According to these results, it can be stated that the earthquake hazard is adequately represented for most of the stations where earthquake accelerations are measured. Determining new values by considering these measured values, especially for stations where the PGA values predicted for the largest earthquake are exceeded, will reveal the effects of earthquakes on structures more realistically. These results once again reveal that the main reason for structural demolitions is that earthquake-resistant building design principles are not taken into account sufficiently during both the construction and design stages. It is seen that in the stations where the largest PGA values were measured for the second earthquake (M_w = 7.6) that occurred on 6 February 2023, the PGA values predicted in the 1996 Türkiye Earthquake Zones Map were exceeded for the Saimbeyli (Adana), Akçadağ (Malatya), and Göksun (Kahramanmaraş) stations, and in other stations, the predicted values met the measured values. It is seen that the PGA values predicted for DD-2, which is the standard design ground motion level in TBEC-2018, exceed the values measured at the Saimbeyli (Adana), Akçadağ (Malatya), and Göksun (Kahramanmaraş) stations. It can be stated that the last two earthquake hazard maps used in Türkiye provide sufficient earthquake hazards for eight stations. For the geographical locations where these three stations are located, a sufficient level of earthquake hazard has been revealed for DD-1, which is the largest earthquake ground motion level. Therefore, earthquake danger is realistically presented in a large part of the earthquake zone. This reveals that the main reason for the demolitions is structural defects. In addition, the occurrence of a second major earthquake 9 h after the first earthquake significantly contributed to the negative impact on structural damage levels.

(**a**)

(**b**)
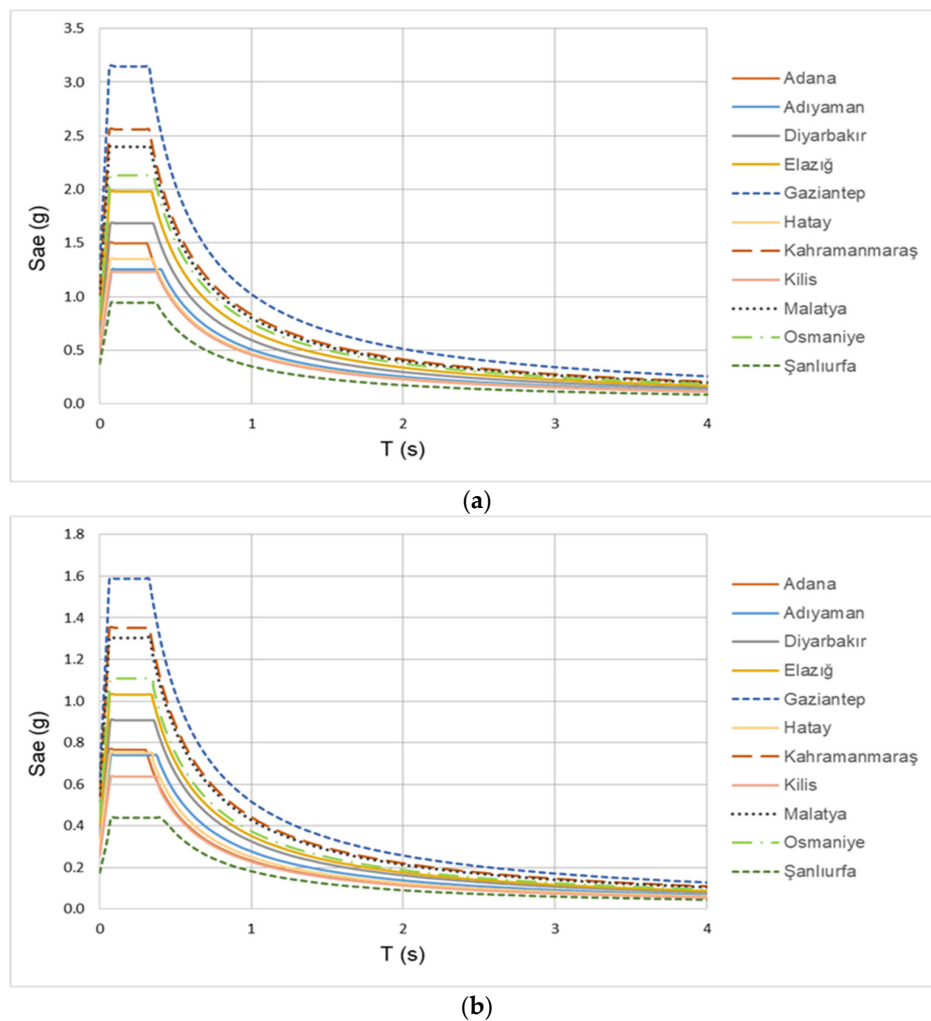
Figure 7. Comparison of the horizontal elastic design spectrums for (**a**) DD-1 and (**b**) DD-2.

5. Results

As a result of the calculations made based on the previously obtained experimental equations and Equation (2) obtained in this study, it was decided that Equation (2), obtained in this study from the comparative graphs drawn in Figures 5 and 6, is the most compatible relation reflecting the intensity distribution in the study area. In addition, it has been seen that the equations [23,37,60,61] given in Table 4 are compatible. The intensity distribution maps created using Equation (2) based on the PGA values recorded for the earthquakes affecting 11 provinces on 6 February 2023 are shown in Figures 8 and 9 for the M_w = 7.7 and M_w = 7.6 earthquakes, respectively. When these maps are compared with intensity distribution maps based on surface observations, it can be seen that there is a significant similarity. Observations based on the effects of an earthquake on the ground and structures can be defined on the intensity scale. These evaluations mostly include personal interpretations. It is very difficult to make such observations for earthquakes with large and widespread effects, such as the one in Kahramanmaraş. Despite this, intensity assessments based on surface observations have mostly been made with high precision. It is understood that ground-based factors are at the root of the compatibility of the maps created based on these data and the maps obtained from the acceleration values in this study. In other words, although construction quality plays an important role in damage, the distribution of the recorded acceleration values revealed the expected intensity distribution and largely overlapped with the resulting damage distribution. In cases affecting compatibility, the non-standard construction factor was effective.
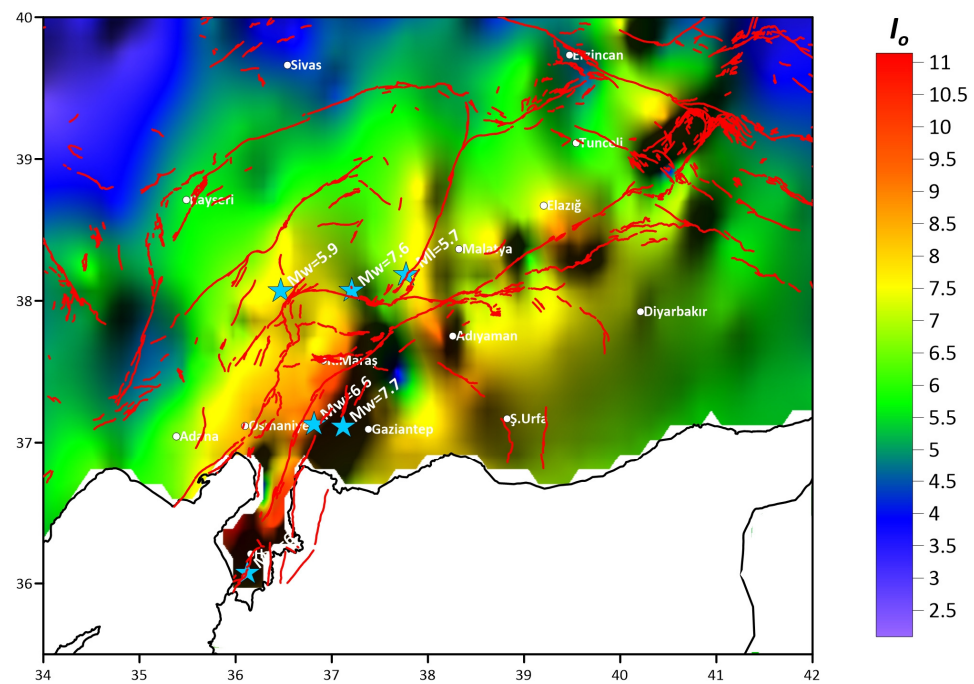
Figure 8. Earthquake intensity distribution map created based on PGA values recorded during the 6 February 2023 Pazarcık–Kahramanmaraş ($M_w = 7.7$) earthquake, the *blue stars* show the locations and magnitudes of the earthquakes.
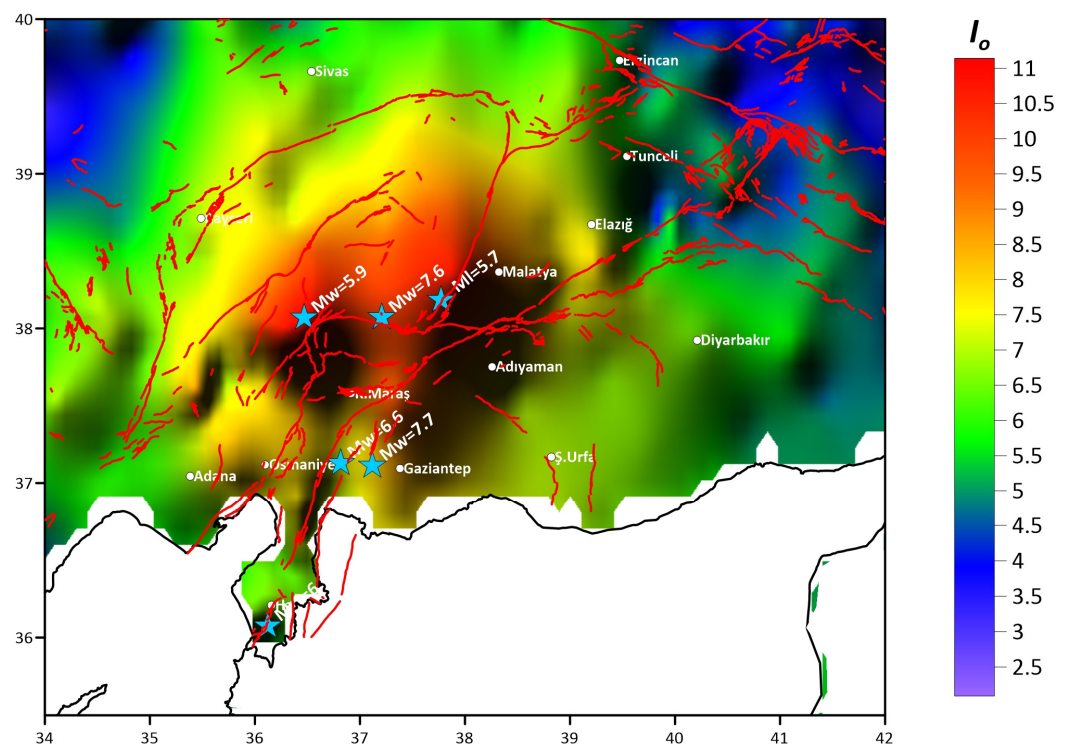
Figure 9. Earthquake intensity distribution map created based on PGA values recorded during the 6 February 2023 Elbistan–Kahramanmaraş ($M_w = 7.6$) earthquake, the *blue stars* show the locations and magnitudes of the earthquakes.

6. Conclusions

Although the intensity of an earthquake increases depending on its magnitude, there are many examples where earthquakes of the same magnitude do not have the same intensity in different geographical locations. In this case, considering the earthquake intensity

scale as a standard all over the world and standardizing the evaluation cannot be a sustainable measurement method and produces statistically misleading results regarding the production of earthquake-resistant buildings. In addition, the effects of ground conditions on buildings are not considered primarily in the intensity distribution or within the framework of the evaluation criteria. Of course, this situation reveals inadequacy in terms of evaluations based on the distribution of earthquake intensity. However, earthquake intensity distribution measurements based on PGA value calculations put forward by many researchers, in which direct ground effects and building negativities can be evaluated together, can provide much more consistent, sustainable, and meaningful earthquake intensity distribution maps.

Within the scope of this study, a PGA–MMI equation was developed according to the acceleration values recorded in the Kahramanmaraş earthquakes on 6 February 2023. Similar equations previously created by different researchers have been compared. Although it was seen that the earthquake intensity increases as the peak ground acceleration (PGA) increases, as expected, it was observed that manufacturing and design errors in buildings play a very important role in the collapses that occur. Intensity distribution maps were created for both earthquakes using the equation developed specifically for Kahramanmaraş earthquakes. While the maximum intensity (Io) of the earthquake was expected to be in the epicenter region, the maximum intensity, M_w = 7.7, specifically for the Pazarcık–Kahramanmaraş earthquake, was seen further south of Antakya. This was the most important indicator that the heavy destruction in Antakya had a ground-based impact. Likewise, the highest intensity value of the Elbistan–Kahramanmaraş earthquake with a magnitude of M_w = 7.6, was observed in the eastern and western settlements. The high PGA values recorded in the same regions confirm these observations. As a result of the on-site earthquake intensity observations and calculations made with the earthquake intensity calculation relations, the maximum intensity (Io) of both earthquakes was XI. Calculations made in this way allow the difference between the expected earthquake intensity and the observed earthquake intensity to be easily distinguished from manufacturing defects that are not related to the ground of buildings or cases where the suitability of the building ground is not considered. On the other hand, the earthquake intensity distribution after an earthquake will be obtained with a very fast, sustainable, and objective method.

References

1. Florido, E.; Aznarte, J.L.; Morales-Esteban, A.; Martínez-Álvarez, F. Earthquake magnitude prediction based on artificial neural networks: A survey. *Croat. Oper. Res. Rev.* **2016**, *7*, 159–169.
2. Hadzima-Nyarko, M.; Pavić, G.; Lešić, M. Seismic vulnerability of old confined masonry buildings in Osijek, Croatia. *Earthq. Struct.* **2016**, *11*, 629–648. [CrossRef]
3. Strukar, K.; Sipos, T.K.; Jelec, M.; Hadzima-Nyarko, M. Efficient damage assessment for selected earthquake records based on spectral matching. *Earthq. Struct.* **2019**, *17*, 271–282.

4. Grünthal, G.; Musson, R.M. Earthquakes, intensity. In *Encyclopedia of Solid Earth Geophysics*; Springer: Cham, Switzerland, 2020; pp. 1–7.

5. Bilgin, H.; Leti, M.; Shehu, R.; Özmen, H.B.; Deringol, A.H.; Ormeni, R. Reflections from the 2019 Durrës Earthquakes: An Earthquake Engineering Evaluation for Masonry Typologies. *Buildings* **2023**, *13*, 2227. [CrossRef]

6. Drei, A.; Milani, G.; Sincraian, G. DEM numerical approach for masonry aqueducts in seismic zone: Two valuable Portuguese examples. *Int. J. Mason. Res. Innov.* **2017**, *2*, 1–29. [CrossRef]

7. Valente, M. Seismic vulnerability assessment and earthquake response of slender historical masonry bell towers in South-East Lombardia. *Eng. Fail. Anal.* **2021**, *129*, 105656. [CrossRef]

8. Wood, H.O.; Newman, F. Modified Mercalli intensity of 1931. *Bull. Seismol. Soc. Am.* **1931**, *21*, 277–283. [CrossRef]

9. Richter, C.F. *Elementary Seismology*; Freeman: San Francisco, CA, USA, 1958; 168p.

10. Shebalin, N.V. Seismic Scale and Methods of Measuring Earthquake Intensity. In *Foci of Strong Earthquakes in the USSR*; IPE AS USSR Publ.: Moscow, Russia, 1978; pp. 87–109. (In Russian)

11. Trifunac, M.D.; Brady, A.G. On the correlation of seismic intensity scale with the peaks of recorded strong ground motion. *Bull. Seismol. Soc. Am.* **1975**, *65*, 139–162.

12. Murphy, J.R.; O'Brien, L.J. The correlation of peak ground acceleration amplitude with seismic intensity and other physical parameters. *Bull. Seismol. Soc. Am.* **1977**, *67*, 877–915. [CrossRef]

13. Trifunac, M.D.; Westermo, B. A note on the correlation of frequency-dependent duration of strong earthquake ground motion with the modified Mercalli intensity and the geologic conditions at the recording stations. *Bull. Seismol. Soc. Am.* **1977**, *67*, 917–927.

14. Hsu, M.T. *Seismology*; Lee-Ming Publication Company: Taipei, Taiwan, 1979; pp. 16–26.

15. McCann, M.; Sauter, F.; Shah, H.C. A technical note on the PGA-intensity relations with applications to damage estimation. *Bull. Seismol. Soc. Am.* **1980**, *70*, 631–637. [CrossRef]

16. Krinitzsky, E.L.; Chang, F.K. Intensity-related earthquake ground motion. *Bull. Int. Assoc. Eng. Geol.* **1988**, *4*, 425–435. [CrossRef]

17. Schenk, V.; Mantlík, F.; Zhizhin, M.N.; Tumarkin, A.G. Relation between macroseismic intensity and instrumental parameters of strong motion –a statistical approach. *Nat. Hazards* **1990**, *3*, 111–124. [CrossRef]

18. Margottini, C.; Molin, D.; Serva, L. Intensity versus ground motion: A new approach using Italian data. *Eng. Geol.* **1992**, *33*, 45–58. [CrossRef]

19. Theodulidis, N.P.; Papazachos, B.C. Dependence of strong ground motion on magnitude-distance, site geology and macroseismic intensity for shallow earthquakes in Greece: I, peak horizontal acceleration, velocity and displacement. *Soil. Dyn. Earthq. Eng.* **1992**, *11*, 387–402. [CrossRef]

20. Theodulidis, N.P.; Papazachos, B.C. Dependence of strong ground motion on magnitude-distance, site geology and macroseismic intensity for shallow earthquakes in Greece: II, horizontal pseudovelocity. *Soil. Dyn. Earthq. Eng.* **1994**, *13*, 317–343. [CrossRef]

21. Panza, G.F.; Cazzaro, R.; Vaccari, F. Correlation between macroseismic intensities and seismic ground motion parameters. *Ann. Geophys.* **1997**, *40*, 1371–1382. [CrossRef]

22. Atkinson, G.M.; Sonley, E. Empirical relationships between Modified Mercalli intensity and response spectra. *Bull. Seismol. Soc. Am.* **2000**, *90*, 537–544. [CrossRef]

23. Boatwright, J.; Thywissen, K.; Seekins, L. Correlation of ground motion and intensity for the 17 January 1994 Northridge, California earthquake. *Bull. Seismol. Soc. Am.* **2001**, *91*, 739–752. [CrossRef]

24. Trifunac, M.D.; Todorovska, M.I. Northridge, California, earthquake of 1994; density of red-tagged buildings versus peak horizontal velocity and intensity of shaking. *Soil Dyn. Earthq. Eng.* **1994**, *16*, 209–222. [CrossRef]

25. Wald, D.J.; Quintoriano, V.; Heaton, T.H.; Kanamori, H. Relationships between peak ground acceleration, peak ground velocity, and Modified Mercalli intensity in California. *Earthq. Spectra* **1999**, *15*, 557–564. [CrossRef]

26. Wald, D.J.; Quintoriano, V.; Heaton, T.H.; Kanamori, H.; Scrivner, C.W.; Worden, C.B. TriNet "ShakeMaps": Rapid generation of peak ground motion and intensity maps for earthquakes in southern California. *Earthq. Spectra* **1999**, *15*, 537–555. [CrossRef]

27. Kaka, S.I.; Atkinson, G.M. Relationships between felt intensity and instrumental ground motion in the central United States and California. *Bull. Seismol. Soc. Am.* **2007**, *97*, 497–510.

28. Worden, C.B.; Gerstenberger, M.C.; Rhoades, D.A.; Wald, D.J. Probabilistic relationships between ground-motion parameters and modified Mercalli intensity in California. *Bull. Seism. Soc. Am.* **2012**, *102*, 204–221. [CrossRef]

29. Karim, K.R.; Yamazaki, F. Correlation of JMA instrumental seismic intensity with strong motion parameters. *Earthq. Eng. Struct. Dyn.* **2002**, *31*, 1191–1212. [CrossRef]

30. Wu, Y.; Teng, T.; Shin, T.; Hsiao, N. Relationship between peak ground acceleration, peak ground velocity, and intensity in Taiwan. *Bull. Seismol. Soc. Am.* **2003**, *93*, 386–396. [CrossRef]

31. Kaka, S.; Atkinson, G. Relationships between instrumental ground-motion parameters and Modified Mercalli intensity in eastern North America. *Bull. Seismol. Soc. Am.* **2004**, *94*, 1728–1736. [CrossRef]

32. Tselentis, G.A.; Danciu, L. Empirical Relationships between Modified Mercalli Intensity and Engineering Ground-Motion Parameters in Greece. *Bull. Seismol. Soc. Am.* **2008**, *98*, 1863–1875. [CrossRef]

33. Gama Garcia, A.; Gomez Bernal, A. Relationships between instrumental ground motion parameters, and modified Mercalli intensity in Guerrero, Mexico. In Proceedings of the 14th World Conference Earthquake Engineering, Beijing, China, 12–17 October 2008.

34. Sørensen, M.B.; Stromeyer, D.; Grünthal, G. Estimation of macroseismic intensity—New attenuation and intensity versus ground motion relations for different parts of Europe. In Proceedings of the 14th World Conference on Earthquake Engineering, Beijing, China, 12–17 October 2008.

35. Linkimer, L. Application of the kriging method to draw isoseismal maps of the significant 2002–2003 Costa Rican earthquakes. *Rev. Geol. Am. Cent.* **2008**, *38*, 119–134. [CrossRef]

36. Faenza, L.; Michelini, A. Regression analysis of MCS intensity and ground motion parameters in Italy and its application in ShakeMap. *Geophys. J. Int.* **2010**, *180*, 1138–1152. [CrossRef]

37. Bayrak, E.; Nas, M.; Bayrak, Y. New macroseismic intensity predictive models for Turkey. *Acta Geophys.* **2019**, *67*, 1483–1513. [CrossRef]

38. Ardeleanu, L.; Neagoe, C.; Ionescu, C. Empirical relationships between macroseimic intensity and instrumental ground motion parameters for the intermediate-depth earthquakes of Vrancea region, Romania. *Nat. Hazards* **2020**, *103*, 2021–2043. [CrossRef]

39. Cilia, M.; Baker, M.L. Ground Motion to Intensity Conversion Equations (GMICEs) for Chilean Megathrust Earthquakes. In Proceedings of the LACSC-SSA 2018 Meeting, Miami, FL, USA, 14–17 May 2018.

40. Hariyanto, T.; Bioresita, F.; Pribadi, C.B.; Safitri, C.N. Determination of Earthquake Intensity Based on PGA (Peak Ground Acceleration) Using Multi-Event Earthquake Data. *IOP Conf. Ser. Earth Environ. Sci.* **2021**, *731*, 012027. [CrossRef]

41. Konovalov, A.; Orlin, I.; Stepnov, A.; Stepnova, Y. Physically Based and Empirical Ground Motion Prediction Equations for Multiple Intensity Measures (PGA, PGV, *Ia*, FIV3, CII, and Maximum Fourier Acceleration Spectra) on Sakhalin Island. *Geosciences* **2023**, *13*, 201. [CrossRef]

42. Anugrayanti, A.; Arsyad, M.; Tiwow, V.A. Analysis of susceptible disaster region based on the peak ground acceleration and earthquake intensity in Mamasa 2018. *J. Phys. Conf. Ser.* **2021**, *1816*, 012014. [CrossRef]

43. Tian, X.; Wen, Z.; Zhang, W.; Yuan, J. New Ground Motion to Intensity Conversion Equations for China. *Shock Vib.* **2021**, *2021*, 5530862. [CrossRef]

44. Available online: https://earthquake.usgs.gov/earthquakes/eventpage/us6000jlqa/shakemap/intensity (accessed on 23 November 2023).

45. Işık, E.; Avcil, F.; Arkan, E.; Büyüksaraç, A.; İzol, R.; Topalan, M. Structural Damage Evaluation of Mosques and Minarets in Adıyaman due to the 06 February 2023 Kahramanmaraş Earthquakes. *Eng. Fail. Anal.* **2023**, *151*, 107345. [CrossRef]

46. Kahya, V.; Genç, A.F.; Sunca, F.; Roudane, B.; Altunişik, A.C.; Yilmaz, S.; Günaydin, M.; Dok, G.; Kirtel, O.; Demir, A.; et al. Evaluation of earthquake-related damages on masonry structures due to the 6 February 2023 Kahramanmaraş-Türkiye earthquakes: A case study for Hatay Governorship Building. *Eng. Fail. Anal.* **2024**, *156*, 107855. [CrossRef]

47. Işık, E. Structural Failures of Adobe Buildings during the February 2023 Kahramanmaraş (Türkiye) Earthquakes. *Appl. Sci.* **2023**, *13*, 8937. [CrossRef]

48. Avcil, F. Investigation of Precast Reinforced Concrete Structures during the 6 February 2023 Türkiye Earthquakes. *Sustainability* **2023**, *15*, 14846. [CrossRef]

49. Karasin, I.B. Comparative Analysis of the 2023 Pazarcık and Elbistan Earthquakes in Diyarbakır. *Buildings* **2023**, *13*, 2474. [CrossRef]

50. İnce, O. Structural damage assessment of reinforced concrete buildings in Adıyaman after Kahramanmaraş (Türkiye) Earthquakes on 6 February 2023. *Eng. Fail. Anal.* **2024**, *156*, 107799. [CrossRef]

51. Ozturk, M.; Arslan, M.H.; Korkmaz, H.H. Effect on RC buildings of 6 February 2023 Turkey earthquake doublets and new doctrines for seismic design. *Eng. Fail. Anal.* **2023**, *153*, 107521. [CrossRef]

52. Zengin, B.; Aydin, F. The Effect of Material Quality on Buildings Moderately and Heavily Damaged by the Kahramanmaraş Earthquakes. *Appl. Sci.* **2023**, *13*, 10668. [CrossRef]

53. Işık, E.; Shendkar, M.R.; Avcil, F.; Büyüksaraç, A.; Deshpande, S.S. A Study on the Determination of Damage Levels in Reinforced Concrete Structures during the Kahramanmaraş Earthquake on February 06, 2023. *E3S Web Conf.* **2023**, *405*, 04029. [CrossRef]

54. Işık, E.; Büyüksaraç, A.; Avcil, F.; Arkan, E.; Ulu, A.E.; Aydin, M.C. Damage evaluation of masonry buildings during Kahramanmaraş (Türkiye) earthquakes on February 06, 2023. *Earthq. Struct.* **2023**, *25*, 209.

55. Zhu, J.; Li, S.; Wei, Y.; Song, J. On-site instrumental seismic intensity prediction for China via recurrent neural network and transfer learning. *J. Asian Earth Sci.* **2023**, *248*, 105610. [CrossRef]

56. Hershberger, J. A comparison of earthquake accelerations with intensity ratings. *Bull. Seismol. Soc. Am.* **1956**, *46*, 317–320. [CrossRef]

57. Sauter, F.; Shah, H.C. *Estudio de Seguro contra Terremoto*; Franz Sauter y Asociados Ltd.: San José, Costa Rica, 1978; 250p.

58. Gallipoli, M.R.; Calamita, G.; Tragni, N.; Pisapia, D.; Lupo, M.; Mucciarelli, M.; Stabile, T.A.; Perrone, A.; Amato, L.; Izzi, F.; et al. Evaluation of soil-building resonance effect in the urban area of the city of Matera (Italy). *Eng. Geol.* **2020**, *272*, 105645. [CrossRef]

59. Gallipoli, M.R.; Mucciarelli, M.; Ponzo, F.; Dolce, M.; D'Alema, E.; Maistrello, M. Buildings as a seismic source: Analysis of a release test at Bagnoli, Italy. *Bull. Seismol. Soc. Am.* **2006**, *96*, 2457–2464. [CrossRef]

60.   Gutenberg, B.; Richter, C.F. Earthquake magnitude, intensity, energy, and acceleration. *Bull. Seismol. Soc. Am.* **1942**, *32*, 163–191. [CrossRef]

61.   Gutenberg, B.; Richter, C.F. Earthquake magnitude, intensity, energy, and acceleration (second paper). *Bull. Seismol. Soc. Am.* **1956**, *46*, 105–145. [CrossRef]